Available online at www.sciencedirect.com
ScienceDirect
International Journal of Heat and Mass Transfer 49 (2006) 4751–4761
International Journal of HEAT and MASS TRANSFER
www.elsevier.com/locate/ijhmt

Direct contact condensation in packed beds

Yi Li, James F. Klausner *, Renwei Mei, Jessica Knight

Department of Mechanical and Aerospace Engineering, University of Florida, Gainesville, FL 32611, United States

Received 29 March 2006; received in revised form 10 June 2006
Available online 1 September 2006

Abstract

A diffusion driven desalination process was recently described where a very effective direct contact condenser with a packed bed is used to condense water vapor out of an air/vapor mixture. A laboratory scale direct contact condenser has been fabricated as a twin tower structure with two stages, co-current and countercurrent. Experiments have been operated in each stage with respective saturated air inlet temperatures of 36, 40 and 43 °C. The temperature and humidity data have been collected at the inlet and exit of the packed bed for different water to air mass flow ratios that vary between 0 and 2.5. A one-dimensional model based on conservation principles has been developed, which predicts the variation of temperature, humidity, and condensation rate through the condenser stages. Agreement between the model and experiments is very good. It is observed that the countercurrent flow stage condensation effectiveness is significantly higher than that for the co-current stage. The condensation heat and mass transfer rates were found to decrease when water blockages occur within the packed bed. Using high-speed digital cinematography, it was observed that this problem can occur at any operating condition, and is dependent on the packing surface wetting characteristics. This observation is used to explain the requirement for two different empirical constants, depending on packing diameter, suggested by Onda for the air side mass transfer coefficient correlation.

Keywords: Condensation; Direct contact; Packed bed; Heat/mass transfer

1. Introduction

A seawater distillation process that has drawn interest over the past two decades is humidification dehumidification desalination (HDH). Numerous investigators, including Bourouni et al. [1], Al-Hallaj et al. [2], Assouad and Lavan [3], Muller-Holst et al. [4], Abdel-Salam et al. [5], Xiong et al. [6], Shaobo et al. [7], Xiong et al. [8], El-Dessouky [9], Goosen et al. [10], and Al-Hallaj and Selman [11] have shown that this process has advantages when operating off of low thermodynamic availability energy such as waste heat. However, they utilize film condensation, which is ineffective in the presence of non-condensable gas, and thus they are not typically cost competitive. Klausner et al. [12,13] recently described an economically feasible diffusion driven desalination (DDD) process to overcome this shortcoming. DDD is a distillation process driven by waste heat derived from low pressure condensing steam within a thermoelectric power plant and is viable for inexpensive large-scale fresh water production (>1 million gallons per day). To enhance the heat transfer rate in the presence of non-condensable gas, a direct contact condenser approach, initially described by Bharathan et al. [14], is utilized. The packed column is well known as an efficient device for gas–liquid direct contact mass transfer such as absorption, stripping, and distillation.

Distillation with the DDD process occurs via humidification of a flowing air stream and dehumidification of that air stream. A characteristic of the DDD process is that the air flow rate through the system is significantly higher than the vapor flow evaporated into the air stream and liquid condensed out. In order for the DDD process to be cost effective, an efficient and low cost method is required to

* Corresponding author. Tel.: +1 352 392 3506; fax: +1 352 392 1071.
E-mail address: klaus@ufl.edu (J.F. Klausner).

0017-9310/$ - see front matter © 2006 Elsevier Ltd. All rights reserved.
doi:10.1016/j.ijheatmasstransfer.2006.06.013

Nomenclature

A	control surface area (m^2)
a	specific area of packing (m^2/m^3)
C_p	specific heat of air (kJ/kg)
d_p	diameter of packing (m)
D	molecular diffusion coefficient (m^2/s)
g	gravity (m/s^2)
G	air mass flux (kg/m^2 s)
h	enthalpy (kJ/kg)
h_{fg}	latent heat of vaporization (kJ/kg)
k	mass transfer coefficient (m/s)
K	thermal conductivity (W/m K)
L	water mass flux (kg/m^2 s)
M_V	vapor molecular weight (kg/kmol)
m	mass flow rate (kg/s)
P	pressure (Pa)
P_{sat}	water vapor saturation pressure (Pa or kPa)
R	universal gas constant (kJ/kmol K)
T	temperature (°C or K)
U	heat transfer coefficient (W/m^2 K)
Φ	relative humidity
ε	condensation effectiveness
μ	dynamic viscosity (kg/m s)
ρ	density (kg/m^3)
σ_L	liquid/gas interfacial surface tension (N/m)
σ_C	critical surface tension of packing (N/m)
ω	absolute humidity

Subscripts

a	air
c	centerline
cond	the portion of liquid condensed
G	air/vapor mixture
GA	gas side parameter based on the specific area of packing
in	inlet condition
L	water in liquid phase
out	exit condition
V	water in vapor phase
x	local value of variable in transverse direction (all the temperatures are bulk temperatures unless denoted by subscript x)

condense water vapor out of the air stream. With a large fraction of the air/vapor mixture being non-condensable, direct contact condensation is considerably more effective than film condensation. In addition, direct contact condensation within a packed bed is more effective than droplet direct contact condensation.

While a significant amount of literature is available on droplet direct contact condensation, considerably less information is available for packed bed direct contact condensation. In analyzing direct contact condensation through packed beds, Jacobs et al. [15] and Kunesh [16] used a volumetric heat transfer coefficient for the rate of convective heat transport and penetration theory [17] to relate the heat and mass transfer coefficient. The volumetric approach does not account for local variations in heat and mass transfer. Penetration theory assumes the liquid behind the interface is stagnant, infinitely deep, and the liquid phase resistance is controlling. As suggested by Jacobs et al. [15] these may or may not be reasonable assumptions, depending on the liquid film condensate resistance. Bharathan and Althof [18] and Bontozoglou and Karabelas [19] improved the analysis of packed bed direct contact condensation by considering conservation of mass and energy applied to a differential control volume. Local heat and mass transfer coefficients were used. Both analyses relied on penetration theory to relate heat and mass transfer coefficients.

The motivation for this work is to experimentally explore the heat and mass transfer process within a packed bed direct contact condenser and develop a robust and reliable predictive model from conservation principles that is useful for design and analysis. A fresh approach is used that does not rely on penetration theory. One of the difficulties encountered is that the interfacial temperature between the liquid and vapor cannot be directly measured, and thus the liquid and vapor heat transfer coefficients cannot be directly measured. Klausner et al. [20] have already developed a detailed evaporative heat and mass transfer analysis for the evaporator section (diffusion tower) of the DDD process. The extensively tested Onda [21] correlation was used to evaluate the mass transfer coefficients on the liquid and gas side. A heat and mass transfer analogy was applied to evaluate the liquid and gas heat transfer coefficients. Excellent results were obtained, and a similar approach will be pursued here.

A laboratory scale packed bed direct contact condenser has been fabricated. The condenser is constructed as a twin tower structure with two stages, co-current and countercurrent. The performance of each stage has been evaluated over a range of flow and thermal conditions. As expected, the countercurrent stage is significantly more effective than the co-current stage. It is found that the manner in which the packing is wetted can significantly influence the heat and mass transfer performance. Visual observations of the wetted packing have been made and a discussion relating the wetting characteristics to the different empirical constants suggested by Onda [21] is provided.

2. Formulation

A physical model is developed for direct contact condensation by considering that cold water is sprayed on top of a

packed bed while hot saturated air is blown through the bed from the bottom. The falling water is captured on the packing surface and forms a thin film in contact with the saturated turbulent air stream. Energy transport during the condensation process is accomplished by a combination of convective heat transfer due to the temperature difference between water and air and the latent heat transport due to vapor condensation. Mass and energy conservation principles govern the condensation of the vapor and the dehumidification of the air stream. Noting that the relative humidity of the air is practically unity during the condensation process, the ideal state of the exit air/vapor temperature from the condenser is close to the water inlet temperature.

A general approach for modeling the flow of water/air through a packed bed is to consider flow through an array of round channels with both transverse and longitudinal variations of temperature, pressure and humidity. This method was applied by Bemer and Kalis [22] in predicting the pressure drop and liquid hold-up of random packed beds consisting of ceramic Raschig rings and metal Pall rings. It was also used by Bravo et al. [23,24] for structured packing. Because the air flow through the packing is highly turbulent, a 1/7th law variation of air temperature in the transverse direction can be assumed [25] as

$$\frac{T_{\mathrm{L}}-T_{\mathrm{a},x}}{T_{\mathrm{L}}-T_{\mathrm{a,c}}}=\left(1-\frac{x}{l}\right)^{1/7}, \tag{1}$$

where $T_{\mathrm{a,c}}$ is the centerline air temperature, T_{L} is the bulk liquid temperature, l is the half width of the hypothetical flow channel, and x is the transverse axis. Although the 1/7th law profile may not be exact, it has proven to be robust in other channel and film flow applications. The centerline air temperature is expressed in terms of the respective bulk air and liquid temperatures as

$$T_{\mathrm{a,c}}=T_{\mathrm{L}}+1.224(T_{\mathrm{a}}-T_{\mathrm{L}}). \tag{2}$$

Eq. (1) is used to evaluate the transverse distribution of air temperature. The local absolute humidity ω_x, based on local transverse air temperature $T_{\mathrm{a},x}$, is related to the relative humidity Φ as

$$\omega_x=\frac{m_{\mathrm{V}}}{m_{\mathrm{a}}}=\frac{0.622\Phi P_{\mathrm{sat}}(T_{\mathrm{a},x})}{P-\Phi P_{\mathrm{sat}}(T_{\mathrm{a},x})}, \tag{3}$$

where P(kPa) is the total system pressure, and P_{sat}(kPa) is the water saturation pressure corresponding to the local air temperature $T_{\mathrm{a},x}$.

The area-averaged humidity ω_{m} at any cross-section is expressed as

$$\omega_{\mathrm{m}}=\frac{2}{l^2}\int_0^l \omega_x x\mathrm{d}x, \tag{4}$$

and the bulk humidity ω at any cross-section is calculated from Eq. (3) based on the air bulk temperature T_{a}, which is a cross-sectional area-averaged value.

A careful examination of the area-averaged humidity and the bulk humidity calculated at the same cross section shows that: for a given total system pressure $P=101.3$ kPa, the air bulk temperature $T_{\mathrm{a}}\leqslant 75$ °C, and the bulk temperature difference between the air and water $|T_{\mathrm{a}}-T_{\mathrm{L}}|\leqslant 20$ °C, the relative difference of the area-averaged humidity and the bulk humidity $\left|\frac{\omega-\omega_{\mathrm{m}}}{\omega_{\mathrm{m}}}\right|\leqslant 1.8\%$. This implies that replacing the area-averaged humidity ω_{m} with the bulk humidity ω will only cause minimal error in predicting the heat and mass transfer rates within the packed bed. Therefore, the bulk humidity is used in the current formulation. This observation allows a one-dimensional treatment of the conservation equations to be used along the z-direction with confidence.

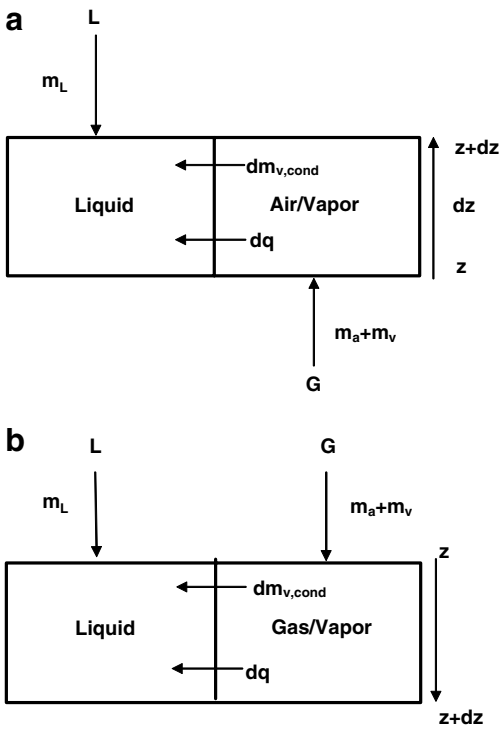

Fig. 1. Differential control volume for liquid/gas heat and mass transfer within a packed bed condenser (a) countercurrent flow and (b) co-current flow.

The current formulation is based on a two-fluid film model in which one-dimensional conservation equations for mass and energy are applied to a differential control volume shown in Fig. 1(a) for countercurrent flow. For this configuration, the air/vapor mixture is blown from bottom to top (z-coordinate). Such an approach has been successfully used by Klausner et al. [20] to model film evaporation in the diffusion tower.

The conservation of mass applied to the liquid and vapor phases of the control volume in Fig. 1(a) results in:

$$\frac{\mathrm{d}}{\mathrm{d}z}(m_{\mathrm{V},z})=\frac{\mathrm{d}}{\mathrm{d}z}(m_{\mathrm{L},z})=-\frac{\mathrm{d}}{\mathrm{d}z}(m_{\mathrm{V,cond}}), \tag{5}$$

where m is the mass flow rate, the subscripts L, V, and cond denote the liquid, vapor, and condensate, respectively. The conservation of energy applied to the liquid phase of the control volume yields:

$$\frac{\mathrm{d}}{\mathrm{d}z}(m_{\mathrm{L}}h_{\mathrm{L}}) = -\frac{\mathrm{d}(m_{\mathrm{V,cond}})}{\mathrm{d}z}h_{\mathrm{fg}} + Ua(T_{\mathrm{L}} - T_{\mathrm{a}})A, \tag{6}$$

where U is the overall heat transfer coefficient and h is the enthalpy. Noting that $\mathrm{d}h_{\mathrm{L}} = C_{p_{\mathrm{L}}}\mathrm{d}T_{\mathrm{L}}$ and combining with Eqs. (5) and (6) results in an expression for the gradient of water temperature in the condenser:

$$\frac{\mathrm{d}T_{\mathrm{L}}}{\mathrm{d}z} = \frac{G}{L}\frac{\mathrm{d}\omega}{\mathrm{d}z}\frac{(h_{\mathrm{fg}} - h_{\mathrm{L}})}{C_{p_{\mathrm{L}}}} + \frac{Ua(T_{\mathrm{L}} - T_{\mathrm{a}})}{C_{p_{\mathrm{L}}}L}, \tag{7}$$

where L is the water mass flux. Eq. (7) is a first order ordinary differential equation with T_{L} being the dependent variable and when solved yields the water temperature distribution through the condenser.

The conservation of energy applied to the air/vapor mixture of the control volume yields:

$$-\frac{\mathrm{d}}{\mathrm{d}z}(m_{\mathrm{a}}h_{\mathrm{a}} + m_{\mathrm{V}}h_{\mathrm{V}}) - \frac{\mathrm{d}(m_{\mathrm{V,cond}})}{\mathrm{d}z}h_{\mathrm{fg}}(T_{\mathrm{a}}) = -Ua(T_{\mathrm{L}} - T_{\mathrm{a}})A. \tag{8}$$

Noting that the specific heat of the air/vapor mixture is evaluated as

$$C_{p_{\mathrm{G}}} = \frac{m_{\mathrm{a}}}{m_{\mathrm{a}} + m_{\mathrm{V}}}C_{pa} + \frac{m_{\mathrm{V}}}{m_{\mathrm{a}} + m_{\mathrm{V}}}C_{p\mathrm{V}} \tag{9}$$

and combining with Eqs. (5) and (8) yields the gradient of air temperature in the condenser,

$$\frac{\mathrm{d}T_{\mathrm{a}}}{\mathrm{d}z} = -\frac{1}{1+\omega}\frac{\mathrm{d}\omega}{\mathrm{d}z}\frac{h_{\mathrm{L}}(T_{\mathrm{a}})}{C_{p_{\mathrm{G}}}} + \frac{Ua(T_{\mathrm{L}} - T_{\mathrm{a}})}{C_{p_{\mathrm{G}}}G(1+\omega)}. \tag{10}$$

Eq. (10) is another first order ordinary differential equation with T_{a} being the dependent variable and when solved yields the air/vapor mixture temperature distribution along the z-direction. Thus Eqs. (7) and (10) are solved simultaneously to evaluate the temperature and humidity fields along the height of the condenser. Since a one-dimensional formulation is used, these equations require closure relationships. Specifically, the humidity gradient and the overall heat transfer coefficient are required.

The bulk humidity, ω, based on air temperature T_{a}, is related to the relative humidity Φ and calculated from Eq. (3). An empirical representation of the saturation curve is

$$P_{\mathrm{sat}}(T) = a\exp(bT - cT^2 + dT^3), \tag{11}$$

where empirical constants are $a = 0.611379$, $b = 0.0723669$, $c = 2.78793 \times 10^{-4}$, $d = 6.76138 \times 10^{-7}$, and T (° C) is the temperature.

Noting that the relative humidity of air remains approximately 100% during the condensation process, the absolute humidity ω is only a function of air temperature T_{a} when the total system pressure P remains constant. Differentiating Eq. (3) with respect to T_{a} and combining with Eq. (11), the gradient of humidity can be expressed as

$$\frac{\mathrm{d}\omega}{\mathrm{d}z} = \frac{\mathrm{d}T_{\mathrm{a}}}{\mathrm{d}z}\frac{P}{P - P_{\mathrm{sat}}(T_{\mathrm{a}})}\omega\left(b - 2cT_{\mathrm{a}} + 3dT_{\mathrm{a}}^2\right). \tag{12}$$

Eqs. (3) and (12) are used in Eqs. (7) and (10) to compute the water and air temperature variation through the condenser for countercurrent flow.

Following the methodology of Klausner et al. [20], the mass transfer coefficients are evaluated using a widely tested correlation and the heat transfer coefficients are evaluated using a heat and mass transfer analogy for the liquid and gas. This approach overcomes the difficulty that gas and liquid heat transfer coefficients cannot be directly measured because the interfacial film temperature is not known. The mass transfer coefficients, k_{L} and k_{G}, associated with film flow in packed beds have been widely investigated. The most widely used and perhaps most reliable correlation is that proposed by Onda et al. [21] as

$$k_{\mathrm{L}} = 0.0051Re_{\mathrm{Lw}}^{2/3}Sc_{\mathrm{L}}^{-0.5}(ad_{\mathrm{p}})^{0.4}\left[\frac{\mu_{\mathrm{L}}g}{\rho_{\mathrm{L}}}\right]^{1/3} \tag{13}$$

and

$$k_{\mathrm{G}} = CRe_{\mathrm{GA}}^{0.7}Sc_{\mathrm{G}}^{1/3}(ad_{\mathrm{p}})^{-2}aD_{\mathrm{G}}\begin{cases} C = 5.23 & \text{for} \quad d_{\mathrm{p}} > 0.015 \\ C = 2.0 & \text{for} \quad d_{\mathrm{p}} \leqslant 0.015 \end{cases}. \tag{14}$$

Definitions of the dimensionless groups in Onda's correlation are listed in the Appendix. As mentioned previously, the heat and mass transfer analogy [26] is used to compute the heat transfer coefficients for the liquid and gas. Therefore the heat transfer coefficients are computed as follows:
Heat transfer coefficient on the liquid side:

$$\frac{Nu_{\mathrm{L}}}{Pr_{\mathrm{L}}^{1/2}} = \frac{Sh_{\mathrm{L}}}{Sc_{\mathrm{L}}^{1/2}}, \tag{15}$$

$$U_{\mathrm{L}} = k_{\mathrm{L}}\left(\rho_{\mathrm{L}}C_{p_{\mathrm{L}}}\frac{K_{\mathrm{L}}}{D_{\mathrm{L}}}\right)^{1/2}. \tag{16}$$

Heat transfer coefficient on the gas side:

$$\frac{Nu_{\mathrm{G}}}{Pr_{\mathrm{G}}^{1/3}} = \frac{Sh_{\mathrm{G}}}{Sc_{\mathrm{G}}^{1/3}}, \tag{17}$$

$$U_{\mathrm{G}} = k_{\mathrm{G}}(\rho_{\mathrm{G}}C_{p_{\mathrm{G}}})^{1/3}\left(\frac{K_{\mathrm{G}}}{D_{\mathrm{G}}}\right)^{2/3}. \tag{18}$$

Overall heat transfer coefficient:

$$U = \left(U_{\mathrm{L}}^{-1} + U_{\mathrm{G}}^{-1}\right)^{-1}. \tag{19}$$

Here K denotes the thermal conductivity and D denotes the molecular diffusion coefficient. Eq. (19) is applied to the one-dimensional conservation equations (Eqs. (7) and (10)) for closure.

A similar mass and energy balance analysis has been done for the co-current flow condenser stage. The one-dimensional conservation equations are applied to a differential control volume shown in Fig. 1(b). The equations for evaluating the humidity gradient and air temperature gradient are the same as that for countercurrent flow. The gradient of water temperature in the co-current flow condenser stage is:

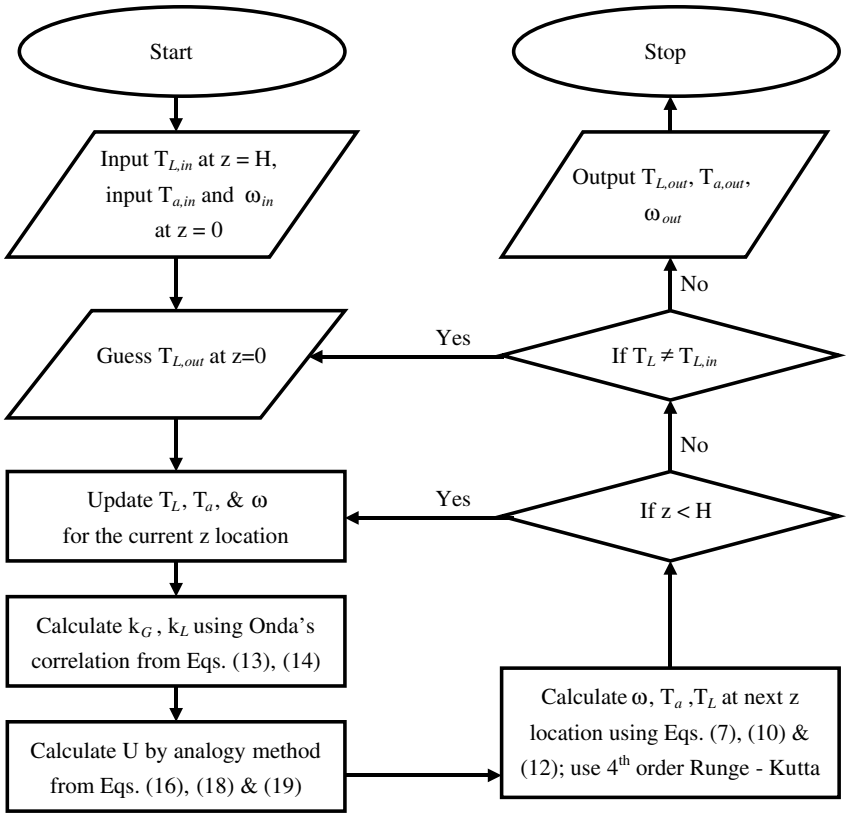

Fig. 2. Flow diagram for the countercurrent flow condenser computation.

$$\frac{dT_L}{dz} = -\frac{G}{L}\frac{d\omega}{dz}\frac{(h_{fg} - h_L)}{C_{p_L}} - \frac{Ua(T_L - T_a)}{C_{p_L}L}. \quad (20)$$

Thus Eqs. (10) and (20) are used to evaluate the temperature fields in the co-current flow condenser stage. The humidity gradient, Onda's correlation and the heat and mass transfer analogy are used for closure.

The condensation rate in the condenser is calculated as

$$m_{cond} = m_a(\omega_{in} - \omega_{out}). \quad (21)$$

The condenser effectiveness is defined as the ratio of the condensation rate in the condenser to the maximum possible condensation rate:

$$\varepsilon = \frac{m_{cond}}{m_a(\omega_{in} - \omega_{sin\,k})}. \quad (22)$$

Here, $\omega_{sin\,k}$ is the minimum possible humidity exiting the condenser, which is evaluated with Eq. (3) assuming the air exits the condenser at the water inlet bulk temperature. The condenser effectiveness is very useful in comparing the performance of the co-current and countercurrent flow condenser stages.

For the countercurrent condensation analysis, the exit water temperature, exit air temperature, and exit humidity are computed using the following procedure: (1) specify the inlet water temperature, $T_{L,in}$, air temperature, $T_{a,in}$, and bulk humidity ω_{in}; (2) guess the exit water temperature $T_{L,out}$; (3) compute the temperatures and humidity at the next step change in height, starting from the bottom of the packed bed, using Eqs. (7), (10) and (12) until the computed packed bed height matches the experimental height; (4) check whether the computed inlet water temperature agrees with the specified inlet water temperature, and stop the computation if agreement is found, otherwise repeat the procedure from step 2. A detailed flow diagram of the computation procedure is illustrated in Fig. 2.

The computation is simpler for the co-current flow condensation analysis. The exit water temperature, exit air temperature, and exit humidity are computed using the following procedure: (1) specify the inlet water temperature, $T_{L,in}$, air temperature, $T_{a,in}$, and bulk humidity ω_{in}; (2) starting from the top of the bed, compute the temperatures and bulk humidity, T_a, T_L, and ω, at the next step change in the z-direction using Eqs. (10), (12) and (20); (3) stop the computation when the computed height matches the experimental height.

3. Experimental facility

In order to test the efficacy of the analytical models described in Section 2, an experimental packed bed direct contact condenser has been fabricated. Fig. 3 shows a pictorial view of the laboratory scale DDD facility, and Fig. 4 provides its schematic diagram. Dry air is drawn into a centrifugal blower equipped with a 1.11 kW motor. The discharge air from the blower flows through a 0.102 m inner diameter vertical PVC pipe in which a thermal

Fig. 3. Pictorial view of the laboratory-scale DDD experiment.

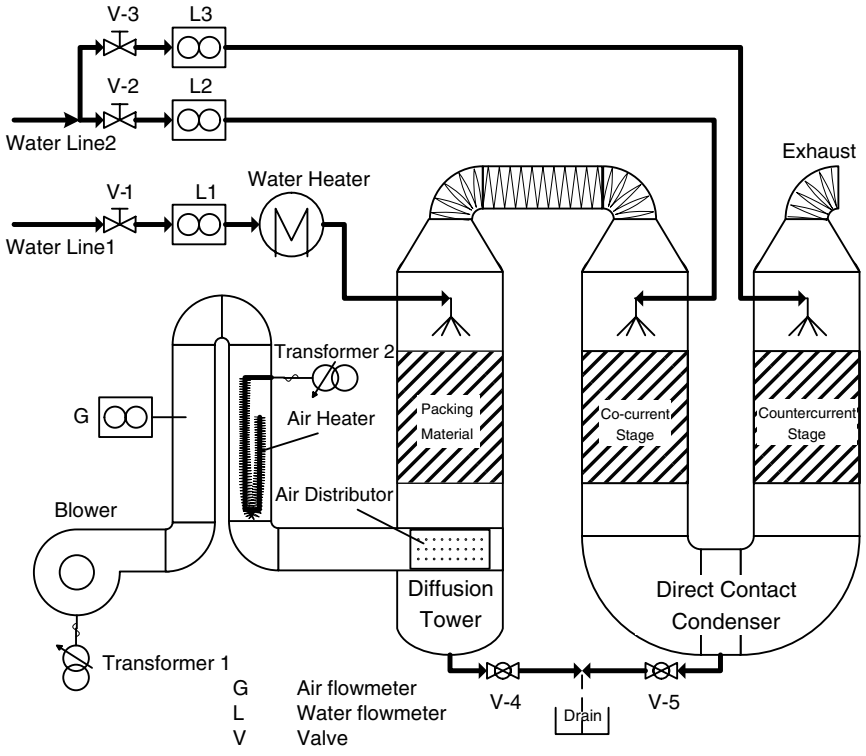

Fig. 4. Schematic diagram of DDD facility.

flowmeter is inserted to measure the air flow rate. Varying the speed of the blower will control the air flow rate. A three-phase autotransformer is used to control the voltage to the blower motor and therefore regulate its speed. Next, the air flows down through a 0.095 m inner diameter CPVC pipe where a 4 kW tubular heater is installed. The amount of power supplied to the heater is regulated by a single-phase autotransformer. The temperature and inlet relative humidity of the air are measured with a thermocouple and a resistance type humidity gauge, downstream of the air heater, in the horizontal section of the air duct. The air is forced through the packing in the diffusion tower where it is heated and humidified by the hot water sprayed in the tower, then discharges through an aluminum duct at the top of the diffusion tower where the temperature and humidity of the discharge air are measured in the same manner as at the inlet. The air exiting the diffusion tower is always saturated for the current investigation. The hot saturated air is then transported to the condenser.

The condenser is comprised of two stages in a twin tower structure. The main feed water, which simulates the cold fresh water, is drawn from a municipal water line and passes through a turbine water flowmeter. After the fresh water temperature is measured at the inlet of the condenser tower by a type-E thermocouple, it is sprayed from the top of each condenser stage.

The hot saturated air forced through the system by the centrifugal blower flows into the co-current stage condenser at its top. The tower body is 0.254 m in diameter and 1.88 m in height. An acrylic section, 0.66 m in length, is used for visual observation. During operation of the countercurrent stage, no cold water is sprayed in the co-current stage, and thus it serves as a well insulated air duct.

The countercurrent stage is connected by PVC elbows to the co-current stage at the bottom where the air and water streams are separated and the air temperature/humidity are measured in the same manner as at the inlet of the diffusion tower. The air is then drawn into the bottom of the countercurrent stage. The tower of the countercurrent stage is identical to the co-current stage. The packing used for the experiments is HD Q-PAC manufactured by Lantec. The HD Q-PAC, constructed from polypropylene, was specially cut using a hotwire so that it snugly fits into the main body of the condenser. The specific area of the packing is 267 m^2/m^3 and its effective packing diameter is 0.017 m. The packing height in the tower was maintained at 0.3 m during experiments. A full cone standard spray nozzle at the tower top provides a water spray that covers nearly the entire cross-section of the condenser. The air will continue being cooled down and dehumidified by the cold water until it is discharged at the top of the countercurrent stage. The exit temperature and humidity of the discharge air are measured in the same manner as at the inlet of the diffusion tower.

A digital data acquisition facility has been developed for measuring the signal output from the experimental facility instrumentation. The data acquisition system consists of a 16-bit analog to digital converter and a multiplexer card with programmable gain manufactured by Computer Boards. A software package, SoftWIRE, which operates in conjunction with MS Visual Basic, allows a user defined graphical interface to be developed for the specific experiment. SoftWIRE facilitates data analysis by recording the data to an Excel spreadsheet.

The measurement uncertainty is $\pm 1.87 \times 10^{-2}$ kg/m^2 s for the water inlet mass flux, $\pm 1.185 \times 10^{-3}$ for the absolute humidity, and $\pm 5.92 \times 10^{-3}$ kg/m^2 s for the air inlet mass flux at 101.3 kPa, 20 °C, and 0% relative humidity. Type-E thermocouples have an estimated uncertainty of ±0.2 °C. Experimental measurements are reported at steady state conditions.

4. Experimental and computational results

The effective packing diameter d_p for the structured polypropylene packing is 0.017 m. In Onda's original work [21] he suggested that the coefficient in Eq. (14) should be $C = 5.23$ for $d_p > 0.015$ m and $C = 2.0$ for $d_p \leqslant 0.015$ m. However, careful scrutiny of the data shows that the change in the coefficient is smooth, and the abrupt change represented by a bimodal coefficient is only an approximation. The 0.017 m effective packing diameter used in this work is very close to the threshold suggested by Onda. Good comparison between the measured data and the model is achieved for co-current and countercurrent flow by following Onda's approximation for $C = 2.0$. Onda did not attempt to explain the physical mechanism for reduced mass transfer rate with smaller packing diameter. We believe that the reduced gas mass transfer coefficient in condensers is due to increased liquid hold-up, which causes liquid bridging and reduced area for mass transfer. The wetting of the packing will be discussed in detail following presentation of the heat and mass transfer data.

4.1. Model comparison with experiments

Heat and mass transfer experiments were carried out in the countercurrent flow stage. The air mass flux G was fixed at 0.6 kg/m^2 s with the water to air mass flow ratio m_L/m_a varying from 0 to 2.5. The saturated air inlet temperature, $T_{a,in}$, was fixed at 36.9, 40.8, and 42.8 °C, respectively. The inlet water temperature was approximately 20 °C. The measured exit humidity ω_{out}, exit air temperature $T_{a,out}$, and exit water temperature $T_{L,out}$ are compared with those predicted with the model for all three different saturated air inlet temperatures in Fig. 5(a)–(c). It is observed that the exit water temperature, exit air temperature and exit humidity all decrease with increasing water mass flux for a specified air mass flux. The comparison between the predicted and measured exit water temperature, exit air temperature and exit humidity agrees very well.

Heat and mass transfer experiments were also carried out in the co-current stage. The saturated air inlet temperature was fixed at 35.5, 39.6, and 42.9 °C for each experiment set. The air mass flux was fixed at 0.6 kg/m^2 s, and the water to air mass flow ratio was varied from 0 to 2.5. The inlet water temperature was approximately 22 °C. Fig. 6(a)–(c) show the measured exit humidity, exit air temperature, and exit water temperature in comparison with those predicted with the model for all three different saturated air inlet temperatures. It is observed that the exit water temperature, exit air temperature and exit humidity all decrease with increasing water to air mass flow ratio. The predicted exit air temperature and exit humidity agree well with the experimental measurements. The computed exit water temperature has the largest deviation, although the error is acceptable for design and analysis applications.

4.2. Condenser effectiveness

In order to compare the packed bed direct contact condensation effectiveness between co-current and countercurrent flow, several sets of experiments have been compiled

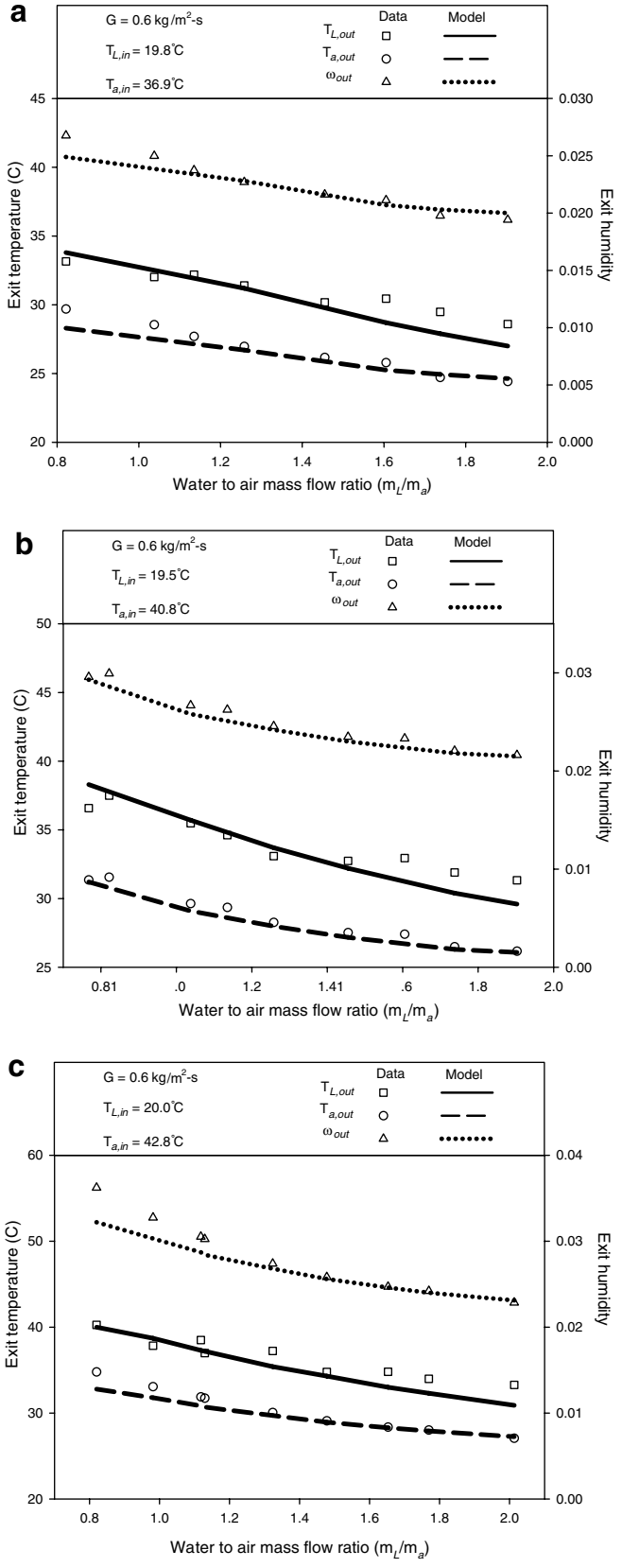

Fig. 5. Comparison of predicted exit temperatures and humidity with the experimental data for countercurrent flow: (a) $T_{a,in} = 36.9$ °C, (b) $T_{a,in} = 40.8$ °C and (c) $T_{a,in} = 42.8$ °C.

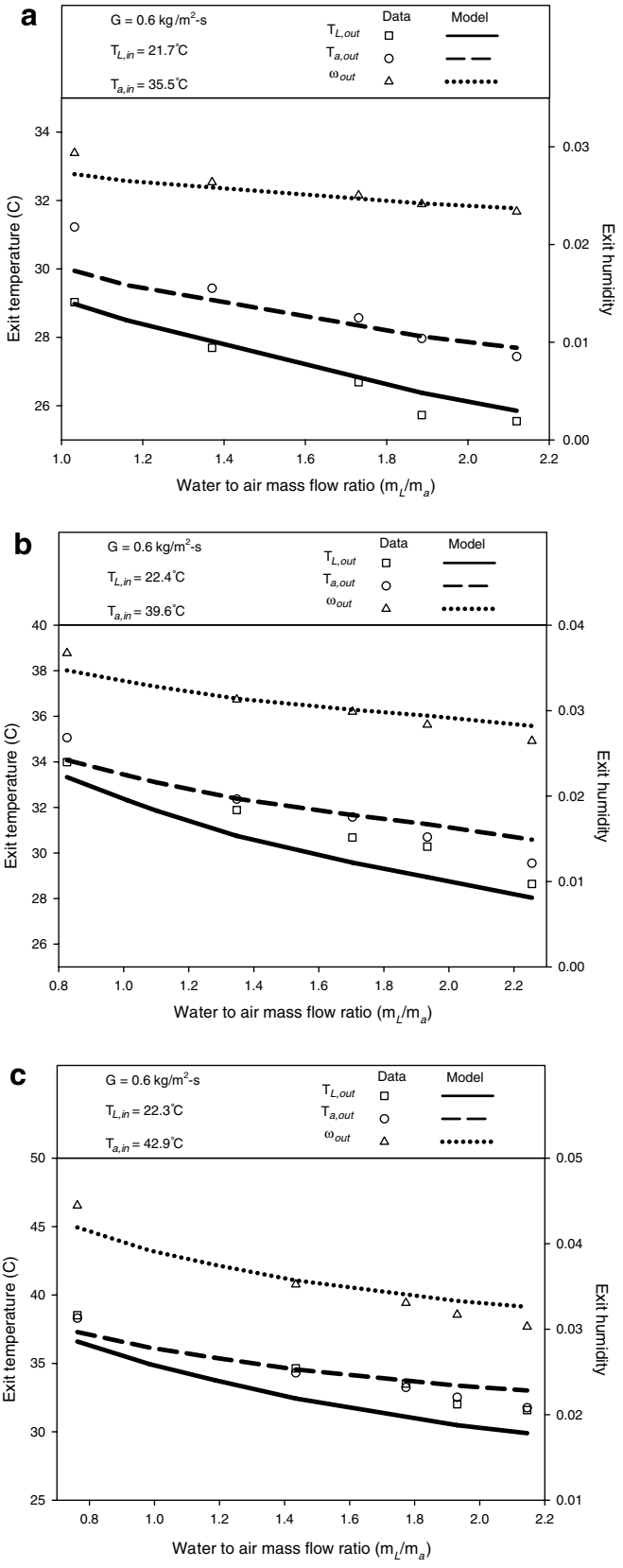

Fig. 6. Comparison of predicted exit temperatures and humidity with the experimental data for co-current flow: (a) $T_{a,in} = 35.5$ °C, (b) $T_{a,in} = 39.6$ °C and (c) $T_{a,in} = 42.9$ °C.

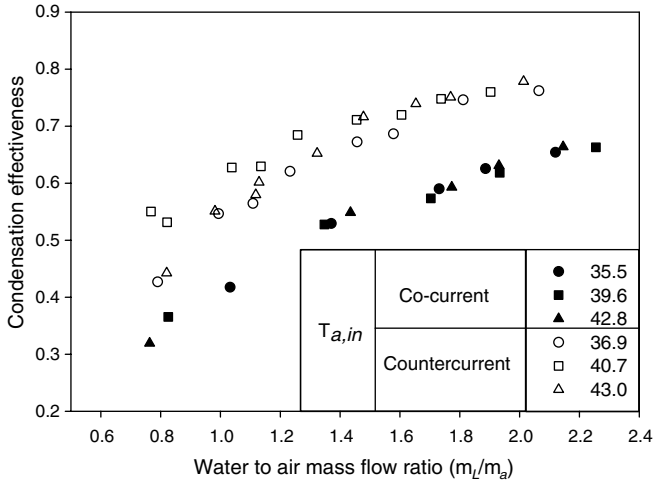

Fig. 7. Comparison of the condenser effectiveness between co-current and countercurrent flow.

where the air flow rate, air inlet temperature/humidity, and water inlet temperature are the same for each condenser stage. The condensation effectiveness is shown in Fig. 7 with varying water to air mass flow ratio at different saturated air inlet temperatures. These data elucidate the fact that the countercurrent flow condenser stage is evidently more effective than the co-current stage for the same water to air mass flow ratio, air inlet temperature/humidity and water inlet temperature. The condensation effectiveness is strongly dependent on the water to air mass flow ratio and not very sensitive to the air inlet temperature/humidity. The condenser effectiveness, for both co-current and countercurrent flow, appears to reach a threshold when the water to air mass flow ratio exceeds 2.0. Operating with this threshold water to air mass flow ratio appears to be an optimal operating condition. In general, the difference between the condenser effectiveness of the co-current and countercurrent stages is approximately 15% for the same water to air mass flow ratio.

4.3. Wetting phenomena

In order to explore the influence of the packing surface wetting on the condensation heat and mass transfer rate, high-speed cinematography was used to study the formation and shape of the liquid film on packing material. A static liquid film formation has been observed when there is no water or air flow through the packed bed and only one droplet of water is on the packing surface. It is found that the water droplet could have three possible residence locations as shown in Figs. 8a–8c. It is also found that the contact angle of water with the polypropylene packing is approximately 90°, which is in agreement with Sellin et al. [27].

Observations of the dynamic water film formation on the packing surface have been made with water and air flowing countercurrently through the packed bed. Frames of the side

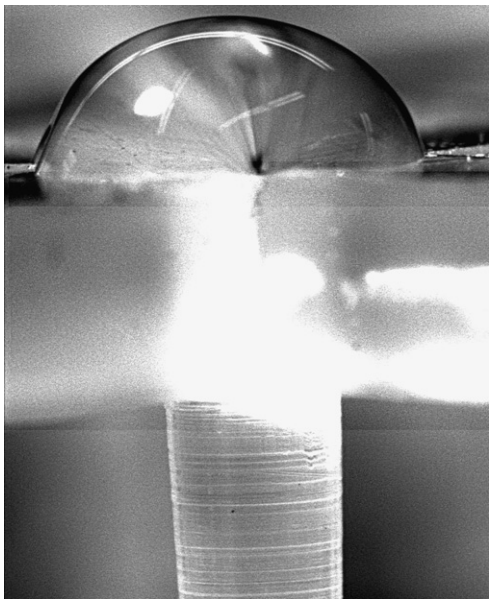

Fig. 8a. Droplet resides on the top of the packing.

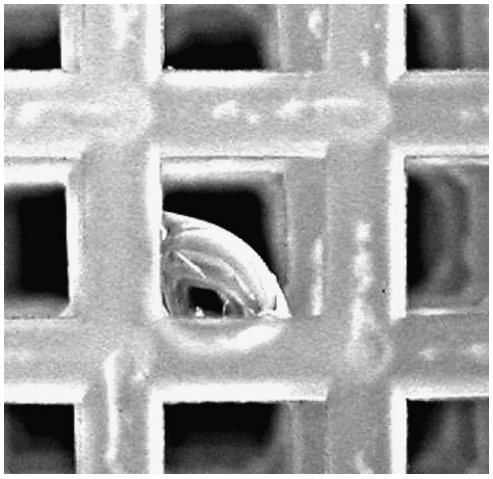

Fig. 8b. Droplet resides in the corner of the packing.

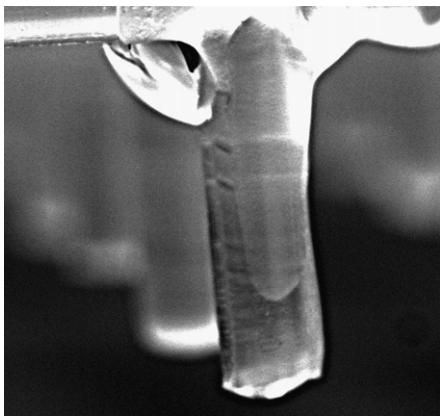

Fig. 8c. Droplet resides beneath the packing.

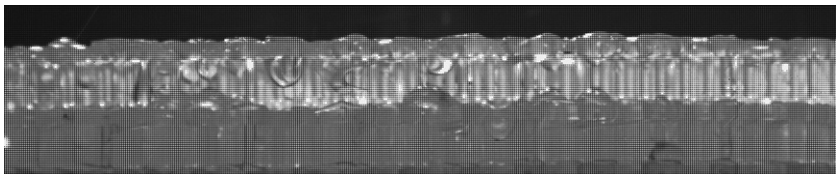

Fig. 9a. Side view of the packed bed.

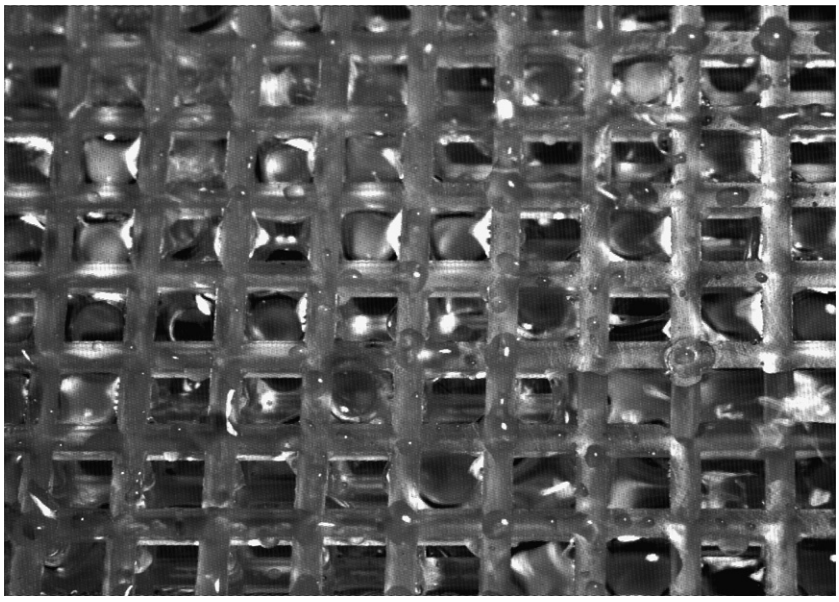

Fig. 9b. Top view of the packed bed.

view and top view are shown in Figs. 9a and 9b, respectively. These images show that some hemispherical water drops block the flow channels within the packed bed. It is observed that the water bridges are always present even at high air to water mass flow ratio. The local heat and mass transfer rate decreases with increasing the water blockages since the active interfacial area between water and air is decreased. Also the air velocity in the vicinity of the blockages is largely reduced due to the increased local flow resistance.

It is well understood that the heat and mass transfer rate within the packed bed is directly related to the contact surface area between the air and water. In order to achieve a high rate of heat and mass transfer, it is important to provide good surface wetting and liquid contact with air. The wettability of the packing surface with liquid depends on the contact angle between the liquid film and the packing surface. Water on polyethylene is poorly wetting. It is apparent that packing material with small packing diameter and poor wettability has a higher probability to form liquid bridges and block the air flow. Also, the condensation process will enhance liquid hold-up and increase the probability of blocking flow passages. This may explain why the local air side heat and mass transfer coefficients are lower for the condensation process than for the evaporation process. Despite its poor wetting characteristics, the polypropylene packing is used for the DDD process because it has a very low cost and is inexpensive to replace.

The wide span of experimental data shown in Onda's original work reveal that there exist more factors important to packed bed heat and mass transfer than are accounted for in the correlation. For example, the water blockage problem on the packing is similar to a local flooding situation, and it could happen at any operating condition depending on the contact angle, packing surface conditions/geometry and heat/mass transfer rate. Predictive models for water blockage are not currently available. Further understanding of liquid flow blockage within packed beds is required to improve existing heat and mass transfer correlations.

5. Conclusion

A laboratory scale direct contact condenser with packed bed has been fabricated with co-current and countercurrent flow stages. Corresponding experiments reveal the heat and mass transfer characteristics for different flow configurations. A comparison between the two stages demonstrates that countercurrent flow generally has 15% higher condensation effectiveness than co-current flow. The condenser effectiveness is strongly dependent on the water to air mass flow ratio and not sensitive to the air inlet temperature/humidity. Because the temperature range is small at any cross section for the current application, a simplified two-fluid model using one-dimensional mass and energy

conservation equations has been developed for co-current and countercurrent flow packed bed direct contact condensation heat and mass transfer. In general, the analytical model proves to be quite satisfactory for predicting the thermal performance of both flow configurations. Nevertheless, due to the empiricism involved in the correlations, it must be used with caution. High-speed cinematography is used to explore the mechanisms for the decrease in the gas side mass transfer coefficient for packing material with a small effective packing diameter. The local heat and mass transfer rate decreases with an increasing number of local water blockages. This is due to a reduction in the active interfacial area between water and air, and the air velocity near the vicinity of the blockages is reduced. It is believed that there exists a higher probability to form liquid blockages within packing material which has a small packing diameter and poor wettability. The analysis and observations presented in this work should be useful to the designers of direct contact condensers.

Acknowledgements

This paper was prepared with the support of the US Department of Energy under Award no. DE-FG26-02NT41537. However, any opinions, findings, conclusions, or recommendations expressed herein are those of the authors and do not necessarily reflect the views of DOE.

Appendix. Onda's correlation

$$k_L = 0.0051 Re_{Lw}^{2/3} Sc_L^{-0.5} (a d_p)^{0.4} \left[\frac{\mu_L g}{\rho_L}\right]^{1/3},$$

$$k_G = C Re_{GA}^{0.7} Sc_G^{1/3} (a d_p)^{-2} a D_G \begin{cases} C = 5.23 & \text{for} \quad d_p > 0.015 \\ C = 2.0 & \text{for} \quad d_p \leqslant 0.015 \end{cases},$$

$$^{\#}a_w = a\left\{1 - \exp\left[-2 \cdot 2\left(\frac{\sigma_c}{\sigma_L}\right)^{3/4} Re_{LA}^{1/2} Fr_L^{-0.05} We_L^{1/5}\right]\right\},$$

$$Re_{LW} = \frac{L}{a_w \mu_L}, \quad Re_{GA} = \frac{G}{a\mu_G}, \quad Re_{LA} = \frac{L}{a\mu_L},$$

$$Sc_L = \frac{\mu_L}{\rho_L D_L}, \quad Sc_G = \frac{\mu_G}{\rho_G D_G}, \quad Fr_L = \frac{L^2 a}{\rho_L g}, \quad We_L = \frac{L^2}{\rho_L \sigma_L a}.$$

[#] This equation has been modified from Onda's original correlation.

References

[1] K. Bourouni, M.T. Chaibi, L. Tadrist, Water desalination by humidification and dehumidification of air: State of the art, Desalination 137 (1–3) (2001) 167–176.
[2] S. Al-Hallaj, M.M. Farid, A.R. Tamimi, Solar desalination with a humidification–dehumidification cycle: Performance of the unit, Desalination 120 (3) (1998) 273–280.
[3] Y. Assouad, Z. Lavan, Solar desalination with latent heat recovery, J. Solar Energy Eng. 110 (1) (1988) 14–16.
[4] H. Muller-Holst, M. Engelhardt, W. Scholkopf, Small-scale thermal seawater desalination simulation and optimization of system design, Desalination 122–123 (1999) 255–262.
[5] M.S. Abdel-Salam, M.M. Hilal, A.F. El-Dib, M.A. Abdel-Monem, Experimental study of humidification–dehumidification desalination system, Energy Sources 15 (3) (1993) 475–490.
[6] R.H. Xiong, S.C. Wang, L.X. Xie, Z. Wang, P.L. Li, Experimental investigation of a baffled shell and tube desalination column using the humidification–dehumidification process, Desalination 180 (1–3) (2005) 253–261.
[7] H. Shaobo, Y. Shengquan, H. Zhang, Performance optimization of solar humidification–dehumidification desalination process using pinch technology, Desalination 183 (1-3) (2005) 143–149.
[8] R.H. Xiong, S.C. Wang, Z. Wang, L.X. Xie, P.L. Li, A.M. Zhu, Experimental investigation of a vertical tubular desalination unit using humidification–dehumidification process, Chin. J. Chem. Eng. 13 (3) (2005) 324–328.
[9] H.T.A. El-Dessouky, Humidification–dehumidification desalination using waste heat from a gas turbine, Desalination 71 (1) (1989) 19–33.
[10] M.F.A. Goosen, S.S. Sablani, C. Paton, J. Perret, A. Al-Nuaimi, I. Haffar, H. Al-Hinai, W.H. Shayya, Solar energy desalination for arid coastal regions: Development of a humidification–dehumidification seawater greenhouse, Solar Energy 75 (2003) 413–419.
[11] Al-Hallaj, S., Selman, J.R. A comprehensive study of solar desalination with a humidification–dehumidification cycle. Middle East Desalination Research Center Report 98-BS-032b, 2002.
[12] J.F. Klausner, Y. Li, M. Darwish, R. Mei, Innovative diffusion driven desalination process, J. Energy Resour. Technol. 126 (3) (2004) 219–225.
[13] Li, Y., Klausner, J.F., Mei, R., Performance characteristics of the diffusion driven desalination process, Int. J. Desalination, in press.
[14] Bharathan, D., Parsons, B.K., Althof, J.A. Direct-contact condensers for open-cycle OTEC applications, National Renewable Energy Laboratory Report SERI/TP-252-3108 for DOE Contract No. DE-AC02-83CH10093, 1988.
[15] Jacobs, H.R., Thomas, K.D., Boehm, R.F. Direct contact condensation of immiscible fluids in packed beds. Presented at Natl. Heat Transfer Conf., 18th San Diego, CA, USA, 1979, ASME pp. 103–110.
[16] J.G. Kunesh, Direct-contact heat transfer from a liquid spray into a condensing vapor, Ind. Eng. Chem. Res. 32 (10) (1993) 2387–2389.
[17] R. Higbie, The rate of absorption of a pure gas into a still liquid during short periods of exposure, Trans. AIChE 31 (1935) 365–389.
[18] Bharathan, D., Althof, J. An experimental study of steam condensation on water in countercurrent flow in presence of inert gas. In: Proc. of ASME, Paper 84-WA/Sol-25, 1984, New Orleans.
[19] V. Bontozoglou, A.J. Karabelas, Direct-contact steam condensation with simultaneous noncondensable gas absorption, AIChE J. 41 (2) (1995) 241–250.
[20] J.F. Klausner, Y. Li, R. Mei, Evaporative heat and mass transfer for the diffusion driven desalination process, J. Heat Mass Transfer 42 (6) (2006) 528–536.
[21] K. Onda, H. Takechi, Y. Okumoto, Mass transfer coefficients between gas and liquid phases in packed columns, J. Chem. Eng. Jpn. 1 (1968) 56–62.
[22] G.G. Bemer, G.A.J. Kalis, A new method to predict hold-up and pressure drop in packed columns, Trans. Inst. Chem. Eng. 56 (1978) 200–204.
[23] J.L. Bravo, J.A. Rocha, J.R. Fair, Mass transfer in gauze packings, Hydrocarbon Process. 64 (1) (1985) 91.
[24] J.L. Bravo, J.A. Rocha, J.R. Fair, Pressure drop in structured packings, Hydrocarbon Process. 56 (3) (1986) 45.
[25] Kays, W.M., Crawford, M.E. Weigand, B. Convective heat and mass transfer, 2005, 34, New York.
[26] E.R.G. Eckert, Analogies to Heat Transfer Processes, in: E.R.G. Eckert, R.J. Goldstein (Eds.), Measurements in Heat Transfer, Hemisphere Publishers, New York, 1976, pp. 397–423.
[27] N. Sellin, J. Sinezio, C. Campos, Surface composition analysis of PP films treated by corona discharge, Mater. Res. 6 (2) (2003) 163–166.